ORIENTATION-BASED SEGMENTATION OF TEXTURED IMAGES BY ENERGY MINIMIZATION

Maria Sagrebin-Mitzel and Til Aach
Institute of Imaging and Computer Vision, RWTH Aachen University, 52056 Aachen, Germany

Keywords: Orientation-based Segmentation, Textured Images, Superimposed Oriented Patterns, Orientation Tensor, Energy Minimization, Graph Cut.

Abstract: We consider textured images, where the textures are composed of different numbers of additively superimposed oriented patterns. Our aim is to develop an energy minimization approach to segment these images into regions according to the number of patterns superimposed. The number of superimposed patterns can be inferred by testing orientation tensors for rank deficiency. In particular, the hypothesis that a local image patch exhibits a given number of superimposed oriented patterns holds if the corresponding orientation tensor is rank deficient by one. The tests can be carried out based on quantities computed from the eigenvalues of the orientation tensors, or equivalently from invariants such as determinant, minors and trace. Direct thresholding of these quantities leads, however, to non-robust segmentation results. We therefore develop energy functions which consist of a data term evaluating tensor rank, and a smoothness term which assesses smoothness of the segmentation results. As the orientation tensors and thus the data term depend on the number of orientations tested for, we derive a hierarchical algorithm for approximate energy minimization using graph cuts. We show the robustness of the approach using both synthetic and real image data.

1 INTRODUCTION

Various problems in the analysis of digital images require the analysis of textured image contents, such as segmentation or classification (Jain and Farrokhnia, 1991; Randen and Husoy, 1999a; Randen and Husoy, 1999b; Liu and Wang, 2003; Lazebnik et al., 2005; Lategahn et al., 2010). Basically texture classification and segmentation deal with the discrimination of regions which contain textures which are distinct according to some criterion, while each region corresponds to a homogeneous texture.

We consider here textures, which are composed of different numbers of additively superimposed oriented patterns. Such textures occur, for instance, in X-ray images of car tires, which contain different numbers of metal gratings superimposing each other (Fig. 1). Our goal is to segment these images into regions according to the number of superimposed patterns. The analysis of orientations is often based on orientation tensors computed from image gradients, such as in (Bigün and Granlund, 1987; Kass and Witkin, 1987; Zenzo, 1986) for single oriented patterns, and in (Aach et al., 2006; Mühlich and Aach, 2009) for multiple orientations. The number of oriented patterns superimposed across a local image patch can then be determined by the rank of these tensors, specifically by testing orientation tensors for rank deficiency. In particular, the assumption that a local image patch exhibits a given number of oriented patterns holds if the corresponding orientation tensor is rank-deficient by one. The tests can thus be performed based on criteria computed from the eigenvalues of the orientations tensors, or from other invariants such as determinants, minors and trace. One approach, taken in (Aach et al., 2006; Mühlich and Aach, 2009) is to sequentially test for one, two and more orientations by hierarchical thresholding of these criteria. Such purely data-driven thresholding, however, is prone to generate isolated decision errors, in particular in more noisy image data. To achieve robust segmentation results, we follow here the approach of deriving energy functions consisting of a data term evaluating tensor rank, and a smoothness term which assesses the smoothness of the image regions. Similarly as above for the thresholding approach, the data term depends on the number of orientations tested for. We therefore develop here a hierarchical algorithm to minimize the energy using graph cuts (Boykov et al., 2001).

In the following, we first review the tensor-based

Sagrebin-Mitzel M. and Aach T..
ORIENTATION-BASED SEGMENTATION OF TEXTURED IMAGES BY ENERGY MINIMIZATION.
DOI: 10.5220/0003839602490258
In *Proceedings of the International Conference on Computer Vision Theory and Applications* (VISAPP-2012), pages 249-258
ISBN: 978-989-8565-03-7

analysis of single and multiple orientations. We then illustrate the hierarchical structure of our general approach. This is followed by a derivation of the data energy terms. On each level of the hierarchy, the corresponding data term is complemented by a smoothness term, specifically the Potts model, to assess region smoothness. The total energy is then approximately minimized by a graph cut algorithm. We evaluate the algorithm qualitatively and quantitatively using both synthetically generated and real image data.

2 ANALYSIS OF SINGLE AND MULTIPLE ORIENTATIONS

Since orientation estimation plays an important role in wide areas like texture analysis, adaptive filtering and image enhancement, a number of different approaches have been proposed. These include among others quadrature filter based methods (Knutsson and Granlund, 1983; Granlund and Knutsson, 1995; Aach et al., 1995), the structure tensor (Förstner, 1986; Zenzo, 1986; Bigün and Granlund, 1987; Kass and Witkin, 1987; Bigün et al., 1991) and its extensions to orientation tensors for multi-oriented patterns (Aach et al., 2006; Mühlich and Aach, 2009), the energy tensor (Felsberg and Granlund, 2004) or the boundary tensor (Köthe, 2003). Yet another alternative, particularly for orientation-adaptive filtering and feature detection by matched filtering, are single-steerable (Freeman and Adelson, 1991; Jacob and Unser, 2004) and multi-steerable filters (Mühlich et al., 2012).

In the following, we summarize the orientation-tensor based approach to orientation analysis, and a hierarchical, purely data-driven procedure for estimating the number of superimposed oriented patterns.

2.1 Single Orientation

The bivariate gray-level image $f(\mathbf{x})$ is said to be oriented in a local region Ω if and only if

$$f(\mathbf{x}) = f(\mathbf{x} + k\mathbf{v}) \;\; \forall k \in \Re \; and \; \forall \mathbf{x}, \mathbf{x} + k\mathbf{v} \in \Omega \qquad (1)$$

where the case of $f(\mathbf{x})$ being constant over Ω is excluded. The unit vector $\mathbf{v} = (\cos\theta, \sin\theta)^T = \mathbf{v}(\theta)$ describes the orientation of $f(\mathbf{x})$ in terms of the angle θ.

Eq. 1 states that a given image is locally constant with respect to $\mathbf{v}$ if its directional derivative $\frac{\partial f}{\partial \mathbf{v}} = \langle \nabla f, \mathbf{v} \rangle$, i.e., the scalar product between the image gradient ∇f and $\mathbf{v}$, is zero for all gradients computed in the neighborhood Ω.

Because of noise in real image data and to allow for slight model violations, one seeks to find the solution of the following equation

$$\theta = \arg \min_{-\pi/2 < \phi \leq \pi/2} \int_\Omega \left(v^T(\theta) \nabla f(x) \right)^2 d\Omega \qquad (2)$$

which leads to the so-called *structure tensor* approach for orientation estimation found in the pioneering work of (Bigün and Granlund, 1987), (Zenzo, 1986), (Kass and Witkin, 1987) and others.

Using the image gradient $\nabla f = (f_x, f_y)^T$, we define the structure tensor $\mathbf{T}^{(1)} : \Re^N \to \Re^{N \times N}$ (where $N = 2$ for bivariate images) as a local integration over the outer product of the gradient

$$\mathbf{T}^{(1)} = \int_\Omega (\nabla f)(\nabla f)^T d\Omega = \int_\Omega \begin{bmatrix} f_x^2 & f_x f_y \\ f_x f_y & f_y^2 \end{bmatrix} d\Omega \qquad (3)$$

If the image signal is perfectly oriented according to (1) over Ω, the structure tensor $\mathbf{T}^{(1)}$ has one zero eigenvalue and $rank(\mathbf{T}^{(1)}) = 1$. In the presence of more than one orientation, both eigenvalues have a high value and $rank(\mathbf{T}^{(1)}) = 2$. Only in the case of $f(\mathbf{x})$ being perfectly constant over Ω, both eigenvalues vanish and $rank(\mathbf{T}^{(1)}) = 0$.

2.2 Higher-order Orientations

As shown in (Aach et al., 2006) and (Mühlich and Aach, 2009) the detection of higher-order oriented structure can be treated in a similar manner. Let the image $f(\mathbf{x})$ be composed from several single oriented signals $f_i(\mathbf{x})$, $i \in [1, 2, ..., M]$ within a local region Ω:

$$f(\mathbf{x}) = \sum_{i=1}^{M} \alpha_i f_i(\mathbf{x}) \;\; \forall \mathbf{x} \in \Omega \qquad (4)$$

where the α_i denote weighting constants.

For $M = 2$, the composite image $f(\mathbf{x})$ then satisfies:

$$\frac{\partial^2 f(\mathbf{x})}{\partial \mathbf{u} \partial \mathbf{v}} = 0 \;\; \forall \mathbf{x} \in \Omega \qquad (5)$$

where the unit vectors $\mathbf{u} = (\cos\theta, \sin\theta)^T = (u_x, u_y)$ and $\mathbf{v} = (\cos\gamma, \sin\gamma)^T = (v_x, v_y)$ denote the orientations of $f_1(x)$ and $f_2(x)$, respectively. In the same way, (5) holds if the oriented patterns occur in mutually exclusive subregions Ω_1 and Ω_2 of Ω at a region boundary according to

$$f(\mathbf{x}) = f_i(\mathbf{x}) \;\; \forall \mathbf{x} \in \Omega_i \qquad (6)$$

where $\bigcup_i \Omega_i = \Omega$ and $\bigcap_i \Omega_i = \emptyset$.

Constraint (5) can be rewritten as the inner product $\mathbf{a}^T \mathbf{g}^{(2)}(\mathbf{x}) = 0 \;\; \forall \mathbf{x} \in \Omega$, where $\mathbf{a}$ is a three-dimensional vector encoding the orientations given by

$$\begin{aligned} \mathbf{a}^T &= (u_x v_x, u_x v_y + u_y v_x, u_y v_y) \\ &= (\cos\theta\cos\gamma, \sin(\theta + \gamma), \sin\theta\sin\gamma) \end{aligned} \qquad (7)$$

and where $\mathbf{g}^{(2)}$ can be viewed as a higher-order gradient given by

$$\mathbf{g}^{(2)} = (f_{xx}, f_{xy}, f_{yy})^T \tag{8}$$

The components of **a** represent the mixed orientation parameters, which, if needed, can be decomposed into the sought orientation angles θ and γ as shown in (Mühlich and Aach, 2009).

Constraint (5) can now be rewritten to

$$Q(\mathbf{a}) = \int_\Omega \left(\mathbf{a}^T\mathbf{g}^{(2)}\right)^2 d\Omega = 0,\ \ \mathbf{a}^T\mathbf{a} > 0. \tag{9}$$

Minimizing this expression subject to the constraint $\mathbf{a}^T\mathbf{a} > 0$ leads again to an eigensystem analysis, this time of the orientation tensor $\mathbf{T}^{(2)}$ defined as follows:

$$\begin{aligned}\mathbf{T}^{(2)} &= \int_\Omega \left(\mathbf{g}^{(2)}\right)\left(\mathbf{g}^{(2)}\right)^T d\Omega \\ &= \int_\Omega \begin{bmatrix} f_{xx}^2 & f_{xx}f_{xy} & f_{xx}f_{yy} \\ f_{xx}f_{xy} & f_{xy}^2 & f_{xy}f_{yy} \\ f_{xx}f_{yy} & f_{xy}f_{yy} & f_{yy}^2 \end{bmatrix} d\Omega\end{aligned} \tag{10}$$

Confidence in the double orientation hypothesis is high if one eigenvalue is small and the other two are large. Moreover, if the image $f(\mathbf{x})$ exhibits two ideal orientations in Ω, one eigenvalue is zero and $rank(\mathbf{T}^{(2)}) = 2$.

In the case of three orientations, $M = 3$ and $\mathbf{g}^{(3)}$ has the form

$$\mathbf{g}^{(3)} = (f_{xxx}, f_{xxy}, f_{xyy}, f_{yyy})^T \tag{11}$$

which leads to the 4×4 orientation tensor $\mathbf{T}^{(3)}$ defined as

$$\mathbf{T}^{(3)} = \int_\Omega \left(\mathbf{g}^{(3)}\right)\left(\mathbf{g}^{(3)}\right)^T d\Omega \tag{12}$$

Again the presence of three different orientations in the image region Ω can be tested for by an eigensystem analysis of the above orientation tensor.

2.3 Hierarchical Orientation Estimation

Following the above discussion, the estimation of a number of superimposed oriented patterns in a single image patch can be achieved by testing the rank of the orientation tensors, which was based above on an eigensystem analysis. For $M \geq 2$, calculating eigenvectors and eigenvalues of a tensor may require iterative numerical methods. To avoid this step, (Mühlich and Aach, 2009) derived a hierarchical algorithm where rank testing employs tensor invariants such as determinant and trace.

The hierarchical testing of the algorithm was achieved by comparing the ratios

$$s_M = \frac{\sqrt[M+1]{\lambda_1^{(M)} \cdots \lambda_{M+1}^{(M)}}}{\sqrt[M]{\frac{1}{M+1}\sum_{i=1}^{M+1} \lambda_1^{(M)} \cdots \lambda_{i-1}^{M} \lambda_{i+1}^{(M)} \cdots \lambda_{M+1}^{M}}} \tag{13}$$

against predefined thresholds ε_M. $\lambda_i^{(M)}$ denotes the i-th eigenvalue of the orientation tensor $\mathbf{T}^{(M)}$. Note that both numerator and denominator can be computed without an eigensystem analysis from quantities such as trace, determinant and minors of the corresponding tensor $\mathbf{T}^{(M)}$. Both the numerator and denominator of s_M can be interpreted as mean eigenvalues, with the numerator being the geometric mean of all eigenvalues. The upper bound for s_M is one, which is reached when all eigenvalues are equal. The lower bound is zero, which is obtained when at least one eigenvalue vanishes.

The procedure for the hierarchical decision making is as follows: Starting with $M = 1$, compute the orientation tensor $\mathbf{T}^{(M)}$ and the value of s_M. If s_M is smaller than the predefined threshold ε_M, mark the region as M-oriented. Otherwise increment M by one and go to the next decision level by computing $\mathbf{T}^{(M+1)}$ and the corresponding value s_{M+1}.

Applying this procedure with $M_{max} = 3$ results in a segmentation of the image into areas with one, two or three orientations, plus a region with more than three orientations. Fig. 1 (a) shows a part of a X-ray image of a tire, revealing its internal metal grating structure. Fig. 1 (b) shows the corresponding region map obtained for $\varepsilon_1 = 0.5$, $\varepsilon_2 = 0.6$ and $\varepsilon_3 = 0.7$, where the area in dark gray represents single orientations, the area in medium gray double orientations and the area in light gray three orientations.

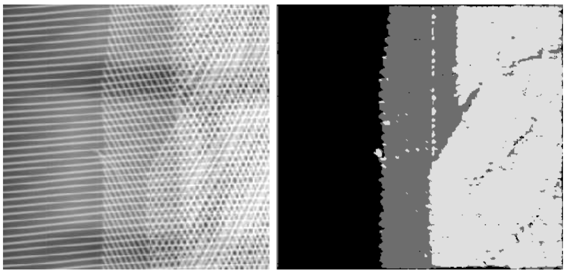

(a) X-ray image of a tire. (b) Segmentation results.

Figure 1: Segmentation results based on the segmentation procedure, proposed by (Mühlich and Aach, 2009).

While the overall estimated region structure corresponds well to the original image, the segmented regions itself are corrupted by small isolated decision errors. On these image parts, a different number of superimposed oriented patterns have been assigned than in the surrounding area.

This behavior is predominantly caused by the fact that each decision considers only local information from the data inside the small image patch Ω. This purely data-driven approach thus ignores region assignments of neighboring image patches. In other words, when making a decision at a specified image patch, no context from decisions for neighboring patches is taken into account (cf. (Besag, 1974; Haralick, 1983; Derin and Cole, 1986; Besag, 1986)).

However, in most applications the assumption of real object being represented through coherent and continuous regions in an image is valid. To incorporate this knowledge into the segmentation procedure, we develop in the following an algorithm which additionally to the data term also uses a regularization term. This additional regularization term imposes further constraints concerning the sought segmentation. It favors segmentation results with coherent larger regions with smooth boundaries rather than small, ragged regions.

The newly developed segmentation algorithm consists of a hierarchy of energy functions, each containing a data and a smoothness term. The definitions of the data terms are based on the ratios defined in (13). The smoothness term is the same in each function.

The hierarchical structure of the proposed approach is described in the next section.

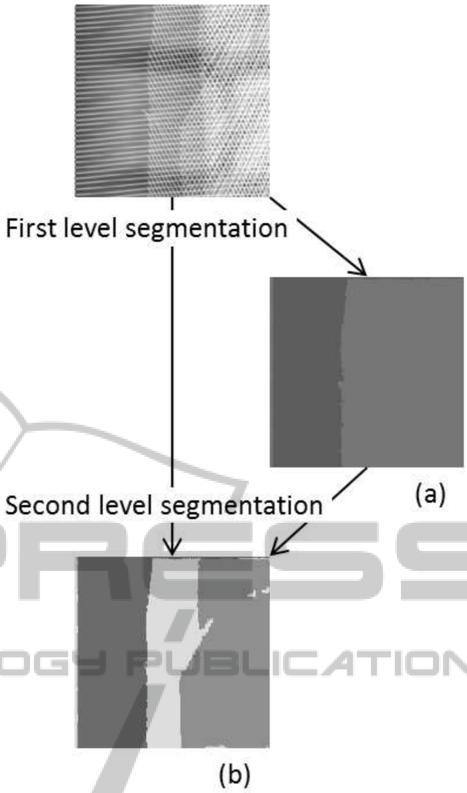

Figure 2: Overview of the approach.

3 APPROACH OVERVIEW

The hierarchical principle of the proposed approach is motivated by the structure of the orientation estimation algorithm discussed in the previous section. On the first level of the hierarchy the image is segmented into two regions corresponding to single and higher order oriented image parts. Further segmentation steps for the second and higher levels of the hierarchy consider only image regions which did not pass the test for a single orientation. Fig. 2 illustrates this procedure exemplarily.

Figs. 2 (a) and (b) show the results of the first and second level segmentation, respectively. In the first step the image is segmented into two regions, where the darker area corresponds to the image region with a single orientation and the brighter area to the image region containing a structure with more than one orientation pattern.

On the second level of the hierarchy, only the image part exhibiting more than one orientation is considered. This region is again divided into two regions, one containing double orientations and the other one containing more than two orientations. The image part with a single oriented structure is disregarded from this step onwards. Following this procedure the segmentation step on the third level of the hierarchy would divide the previously determined higher order oriented image part again into two regions corresponding to image areas with three orientations and those with more than three superimposed patterns.

On every level of the hierarchy, the segmentation is based on a minimization of a level dependent energy function. The data term of these functions incorporates the ratio s_M defined in (13), where M corresponds to the level of the hierarchy. The regularization term is the same in all functions and imposes smoothness constraints on the segmentation results.

To not disturb the neighborhood relationships between adjacent regions, all energy functions of the developed approach are defined over P, which is the set of all image pixels. When testing for a specified number of orientations at the corresponding level of the hierarchy, all regions with a lower number of orientations should be left unchanged. This is achieved by an appropriate definition of the energy function at each level of the hierarchy.

4 ENERGY FUNCTIONS

The segmentation on each level of the hierarchy is based on a minimization of an energy function via graph cuts. The basic idea behind this technique is the construction of a graph such that the minimum cut on the graph also minimizes the corresponding energy function (Boykov et al., 2001). Here, the optimal segmentation of the underlying image is computed by using the *expansion* algorithm, developed by (Boykov et al., 2001). The energy functions they consider in their work have the form

$$E(l) = E_{data}(l) + E_{smooth}(l) \tag{14}$$

where l denotes the labeling of the observed data. For image segmentation, l is a function which assigns to each pixel $p \in P$ the corresponding label $l_p \in L$. The form of $E_{data}(l)$ is given by

$$E_{data}(l) = \sum_{p \in P} D_p(l_p) \tag{15}$$

where D_p measures how well label l_p fits the pixel p. $E_{smooth}(l)$ is the smoothness term of the energy function and measures the extent to which the labeling function l is not piecewise smooth. $E_{smooth}(l)$ has the form

$$E_{smooth}(l) = \sum_{\{p,q\} \in N} V_{p,q}(l_p, l_q) \tag{16}$$

where N is the set of adjacent pairs of pixels and $V_{p,q}(l_p, l_q)$ denotes the penalty for pixels p and q having different labels.

The *expansion* algorithm seeks to find an optimal labeling l^* such that the energy function given in (14) is minimized. It starts with an initial labeling and *moves* in every step toward the labeling with a lower energy until it reaches its minimum. In this context a new labeling l^{new} is said to lie within a single α-*expansion move* of l if only a finite set of pixels have changed their labels to α, where $\alpha \in L$. For more details on this approach, see (Boykov et al., 2001).

The main task is now the definition of appropriate functions $E_h(l)$, $h \in [1, \cdots, h_{max}]$ where h denotes the segmentation level.

As already stated above, all energy functions in our approach have the same smoothness term $E_{smooth}(l)$. Here we have used the Potts model (Potts, 1952) as a discontinuity preserving function:

$$V(\alpha, \beta) = K \cdot T(\alpha \neq \beta) \tag{17}$$

where $T(\cdot)$ is 1 if its argument is true and otherwise 0. This model encourages partitions consisting of larger, smoothly shaped regions.

The definition of the corresponding data terms $E_{data}(l)$ is given in the next sections.

4.1 First-order Data Term

As stated above, the data term $E_{data}(l)$ of an energy function measures how well the given labeling l fits the underlying image data. To obtain such an initial labeling, from which the necessary parameters can be estimated as well as to derive an appropriate data term, we applied the fuzzy c-means algorithm (Bezdek, 1981) to the ratios $s_{M=1}(p)$, $p \in P$ defined in (13), where p denotes the center of the image region Ω.

Fig. 3 shows the spatial distribution and the corresponding histogram of the $s_{M=1}(p)$ values computed from the original image shown in Fig. 1 (a).

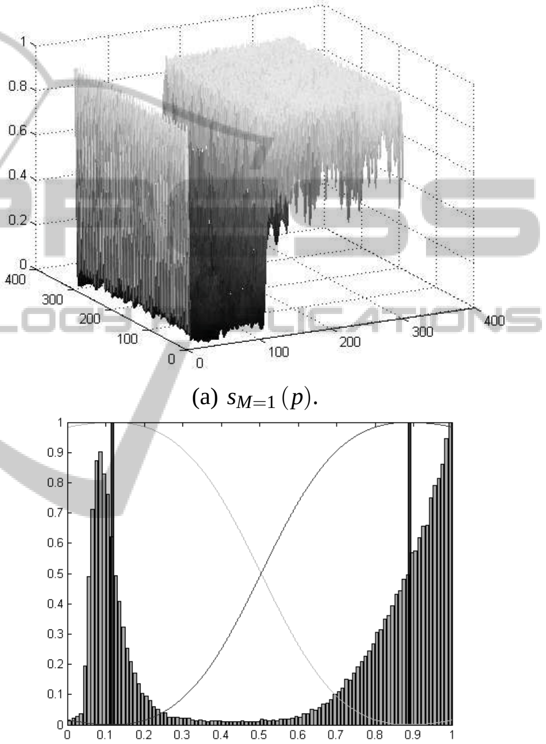

(a) $s_{M=1}(p)$.

(b) Histogram.

Figure 3: Spatial distribution of the ratios $s_{M=1}(p)$, $p \in P$ and the corresponding histogram with cluster centers and membership functions.

Evidently, large values of $s_{M=1}(p)$ indicate a multiple oriented structure in an image, whereas small values correspond to image areas with a single orientation. The histogram in Fig. 3(b) reflects this situation by two clearly separable clusters.

Since in this context the order of the labeling set is $|L| = 2$, we apply the fuzzy c-means algorithm to separate the values into two clusters, which correspond to the labels l^{single} and l^{multi}, respectively. The results of this clustering procedure are also shown in Fig. 3(b). The two black bars correspond to the positions of the computed centers, while the curves depict the membership functions μ^{single} and μ^{multi} of the respective cluster:

$$\begin{array}{l} \mu^{single}\left(s_{M=1}\left(p\right)\right):\ P \rightarrow [0,1] \\ \mu^{multi}\left(s_{M=1}\left(p\right)\right):\ P \rightarrow [0,1] \end{array} \tag{18}$$

The results of a membership function are numerical values in $[0,1]$ that correspond to the degrees to which the pixel $p \in P$ belongs to one or the other cluster. A large value complies with a high degree of affiliation to the corresponding cluster.

We can now define the data term $E_{data}\left(l\right)$ of the first energy function to

$$E_{data}\left(l\right) = \sum_{p \in P}\left(1 - \mu^{l_p}\left(s_{M=1}\left(p\right)\right)\right) \tag{19}$$

where

$$D_p\left(l_p\right) = \left(1 - \mu^{l_p}\left(s_{M=1}\left(p\right)\right)\right) \tag{20}$$

measures how well the label l_p fits the pixel p. Since we seek to minimize the overall energy function, a good fit is represented by a small value.

4.2 Second-order Data Term

The data term $E_{data}\left(l\right)$ of the second level energy function is obtained similarly, with the fuzzy c-means algorithm now being applied to the values $s_{M=2}\left(p\right),\ p \in P$, where again p denotes the center of the image region Ω. Fig. 4 shows the spatial distribution and the corresponding histogram of the $s_{M=2}\left(p\right)$ values computed from the original image shown in Fig. 1 (a). As one can see, the $s_{M=2}\left(p\right)$ values have been computed only for pixels which have been marked as belonging to the image area of multiple orientations, $p \in \Omega^{multi} \subset P$. Pixels of the single oriented image part, $p \in \Omega^{single} \subset P$, have been disregarded in this step. The corresponding histogram shows that in contrast to the $s_{M=1}$ histogram, the two main clusters are here much closer to each other, having their centers around 0.53 and 0.85, respectively.

Application of the fuzzy c-means to these values results in two clusters and two membership functions μ^{double} and μ^{multi}, which in this case correspond to the labels l^{double} and l^{multi}, respectively.

To take into acount the neighborhood relationships between the two regions Ω^{multi} and Ω^{single}, the energy function $E_{h=2}\left(l\right)$ is defined over the entire pixel set P. To leave Ω^{single} unchanged during this and the following segmentation steps, this region is considered as being labeled by a fixed label l^{img}, where the corresponding membership function is defined as:

$$\mu^{img}\left(p\right) = \left\{\begin{array}{l} 1,\ p \in \Omega^{single} \\ 0,\ p \in \Omega^{multi} \end{array}\right\} \tag{21}$$

Additionally, the two membership functions μ^{double} and μ^{multi} are modified according to

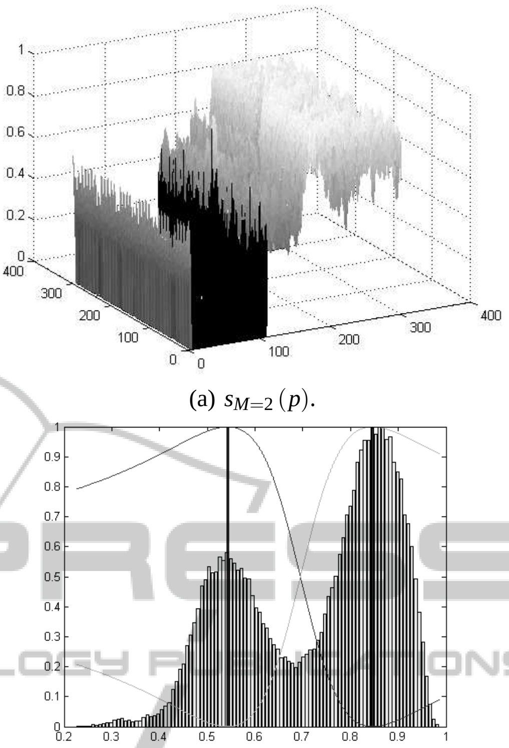

(a) $s_{M=2}\left(p\right)$.

(b) Histogram.

Figure 4: Spatial distribution of the values $s_{M=2}\left(p\right)$ and the corresponding histogram with cluster centers and membership functions.

$$\mu^{double\_mod}\left(p\right) = \left\{\begin{array}{ll} 0 & , p \in \Omega^{single} \\ \mu^{double}\left(s_{M=2}\left(p\right)\right) & , p \in \Omega^{multi} \end{array}\right\}$$

$$\mu^{multi\_mod}\left(p\right) = \left\{\begin{array}{ll} 0 & , p \in \Omega^{single} \\ \mu^{multi}\left(s_{M=2}\left(p\right)\right) & , p \in \Omega^{multi} \end{array}\right\} \tag{22}$$

With these membership functions, the data term $E_{data}\left(l\right)$ of the second level energy function can be defined similarly to that of the first level energy function. Adding the third fixed label with the above defined membership function (21) ensures that the *expansion* algorithm does not relabel the single oriented region and treats the neighborhood relationships of the two regions Ω^{single} and Ω^{multi} in the same manner as inside these regions.

4.3 Higher-order Data Terms

The data term of the higher-order energy function $E_h\left(l\right),\ h \in [3,\cdots,h_{max}]$ is defined in analogy to that of the second order data term. After computing the membership functions of the two labels l^h and l^{multi}, the support of the fixed label l^{img} is extended to cover all regions with an already detected number of orientations, with membership function

$$\mu^{img}(p) = \left\{ \begin{array}{l} 1,\ p \in \Omega^{h-1} \\ 0,\ p \in \Omega^{multi} \end{array} \right\}$$

where in the case of $h = 3$ the image region Ω^{h-1} is a union of the two image regions Ω^{single} and Ω^{double}. Here, Ω^{double} denotes the image region which was labeled as being double oriented in the previous hierarchy level.

The two membership functions μ^{h} and μ^{multi} are also modified in analogy to (22):

$$\mu^{h\_mod}(p) = \left\{ \begin{array}{cl} 0 & ,p \in \Omega^{h-1} \\ \mu^{h}(s_{M=h}(p)) & ,p \in \Omega^{multi} \end{array} \right\}$$

$$\mu^{multi\_mod}(p) = \left\{ \begin{array}{cl} 0 & ,p \in \Omega^{h-1} \\ \mu^{multi}(s_{M=h}(p)) & ,p \in \Omega^{multi} \end{array} \right\}$$

As one can see the ratios s_M are also computed depending on the hierarchy level.

5 EXPERIMENTS AND RESULTS

To test the performance and robustness of the described algorithm quantitatively and qualitatively, we applied it to both synthetic and real image data to detect up to three orientations. The regularization parameter K in (17) was set to $K = 1$ in all cases. Fig. 5 b) shows the segmentation result for the synthetically generated image shown in Fig. 5 a).

This synthetic image contains several parts, each with a different number of superimposed oriented patterns. The structure consists of two additive orientations in each of the two larger rectangles, whereas in the two smaller rectangles the number of superimposed oriented patterns is three. The background of the image is single-oriented.

Evidently, the algorithm segments the image well into three different types of regions. The black area represents the single-oriented image part. The area in dark gray represents image regions where two different orientations have been detected, and the area in medium gray corresponds to image regions containing structures with three different orientations. At the boundary between the double-oriented regions and the single-oriented background, the algorithm detects three occludingly superimposed orientations, also represented by medium gray.

This segmentation result was obtained on the image to which no noise was added. Decreasing the signal-to-noise ratio (SNR) leads first to segmentation results where the mentioned border region around the double-oriented image parts starts to vanish. The uniformity of the regions is disturbed only when the SNR is as low as $SNR = 3dB$. Fig. 6 shows the segmentation results obtained by three different approaches including the one presented in this work.

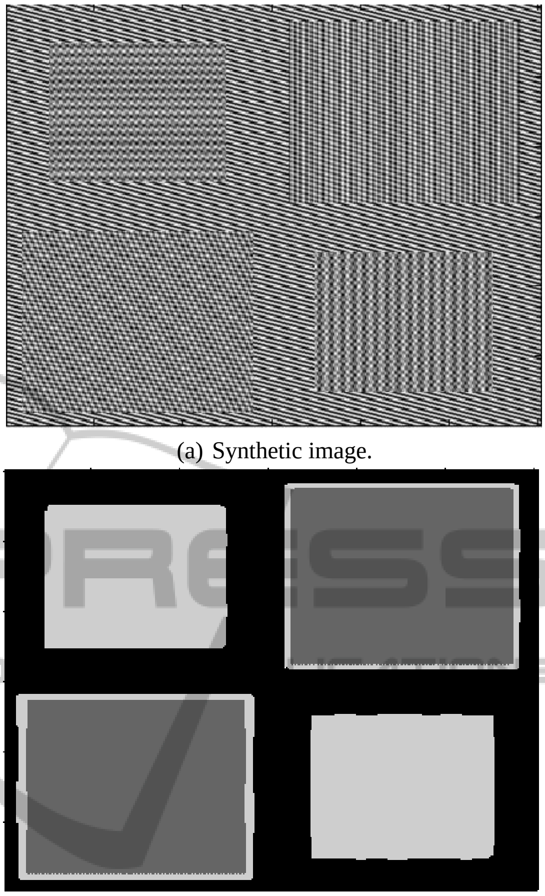
(a) Synthetic image.

(b) Segmentation results.

Figure 5: Segmentation result for the synthetic image with several multi-oriented regions. No noise was added to the image.

Evidently, the described approach produces more stable results than the segmentation procedure based solely on the comparison of the ratios in (13) with the predefined thresholds, as a comparison between Figs. 6 (a) and (b) shows. In Fig. 6 (b), only image parts with three different orientations were segmented properly. The rest of the image contains many misclassified regions. The subsequent application of the *expansion* algorithm to these data, shown in Fig. 6 (c), could not reach the performance of our approach. The initial labeling for the *expansion* algorithm was in this case obtained by the hierarchical thresholding algorithm developed in (Mühlich and Aach, 2009).

Additionally, Fig. 7 shows the development of the F-score values (Frakes, 1992) computed from the segmentation results while decreasing the SNR value of the original image shown in Fig. 5 (a). The F-

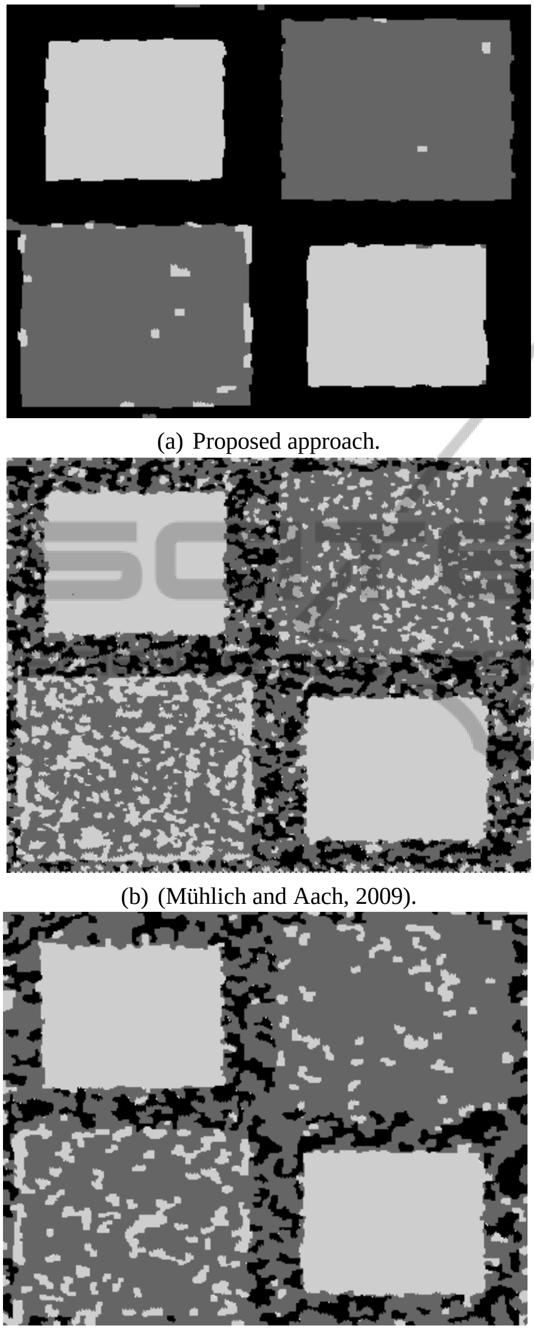

(a) Proposed approach.

(b) (Mühlich and Aach, 2009).

(c) (Mühlich and Aach, 2009) + GraphCut.

Figure 6: Segmentation results for the synthetic image with added noise ($SNR = 3dB$).

score is a measure of the segmentation accuracy. It is computed from precision p and recall r via $F = 2 \cdot (pr)/(p+r)$. Each one of the three plots in Fig. 7 shows three different F-curves corresponding to the segmentation accuracy of the single-, double- and triple-oriented image parts, respectively.

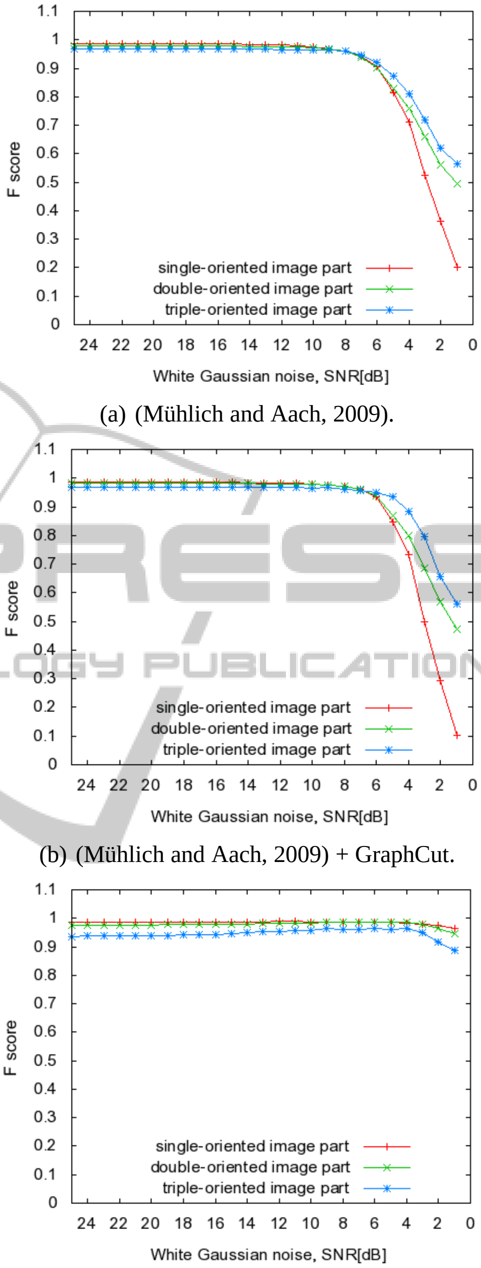

(a) (Mühlich and Aach, 2009).

(b) (Mühlich and Aach, 2009) + GraphCut.

(c) Proposed approach.

Figure 7: F-score computed from the segmentation results while decreasing the SNR value of the original image.

Obviously, SNR-values lower than 8 dB result in a very poor segmentation when using the thresholding procedure in (Mühlich and Aach, 2009). Subsequent application of a graph cut optimization technique could not improve these results substantially. However, the F-score values shown in the third plot testify that the segmentation results obtained with the algorithm developed in this paper are significantly better. Another interesting point is the behavior of the different F-curves relative to each other. In the first two plots the F-curves corresponding to the single oriented image parts decline faster than the other two curves of the same plot. However, in the third plot the F-curve corresponding to the triple oriented image part declines faster, meaning that the segmentation accuracy of the corresponding image regions is getting worse. The following two facts are responsible for this behavior. Adding Gaussian noise to the image tends to lead to higher values of the ratio defined in (13). Thresholding these values by the same threshold leads therefore to a segmentation with more image regions which have been assigned a double-oriented structure. Since we used in our approach an adaptive fuzzy c-means algorithm for the initial cluster labeling, no declining of the red F-curve can be observed in the third plot. Still, experiments have shown that the distance between the two clusters varies strongly depending on which hierarchy level the segmentation is performed. On the first level the distance is relatively large, meaning that the centers lie in $[0, 0.5]$ and $[0.5, 1]$ interval, respectively. On the second level, both cluster centers were in $[0.5, 1]$ interval, which is the main reason for the poor segmentation of the higher-order oriented image structures.

We tested our algorithm also on texture images. In Fig. 8, the original image is composed of three different textures. Both the background texture and the texture on the lower part of the image were taken from the Brodatz database. The resulting segmentation is shown in Fig. 8 (b). It consists of two classes corresponding to single- and multi-oriented image regions, respectively.

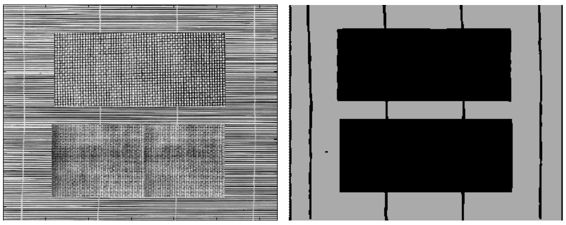
(a) Textured image. (b) Segmentation results.

Figure 8: Segmentation results of the textured image with several multi-oriented regions.

Further results are provided in Fig. 9, where the proposed segmentation approach could robustly separate single- and multi-oriented regions.

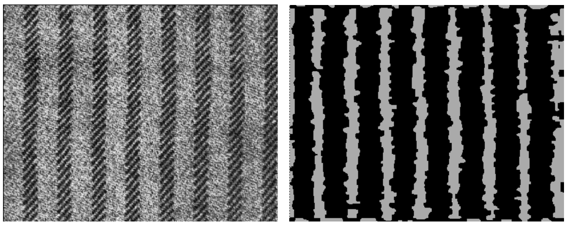
(a) Textured image. (b) Segmentation results.

Figure 9: Segmentation results of the textured image taken from the Brodatz database.

6 CONCLUSIONS

We have developed a hierarchical segmentation algorithm, which separates an image into different regions based on the number of superimposed oriented patterns within each region. The algorithm combines the tensor-based analysis of multiple oriented patterns in (Aach et al., 2006; Mühlich and Aach, 2009) with a Potts region model (Potts, 1952) and energy minimization via graph cuts (Boykov et al., 2001). On every level of the hierarchy, the segmentation is thus achieved through a minimization of the corresponding energy function. The data term of the energy function evaluates the hypothesis that a given image part exhibits a particular number of superimposed orientations, and employs criteria testing the rank of the corresponding orientation tensor. The data term is complemented by a smoothness term derived from the Potts model, which serves as a regularization term. The smoothness energy acts as a discontinuity preserving term, encouraging labellings where adjacent pixels exhibit identical labels except across region boundaries. The energy functions were minimized via graph cuts. The algorithm was evaluated quantitatively and qualitatively on both synthetic and real image data. The quantitative evaluation verified the robustness of the algorithm against image noise in signal-to-noise ratios as low as $3dB$. Similarly, a strong performance of the algorithm was observed in real image data, such as textures and texture mosaics from the Brodatz database. In particular, the occurrence of isolated segmentation errors could be significantly reduced in comparison to the non-regularized thresholding approaches in (Mühlich and Aach, 2009).

We concentrated here on the segmentation of single- and multi-oriented textures according to the number of oriented patterns present in a region. We therefore did intentionally not consider the orientations themselves, which are encoded in the eigenvectors (particularly in the eigenvector corresponding to the lowest eigenvalue of an orientation tensor) rather than the eigenvalues. Future work is directed at including explicit orientation information into the framework, thus allowing to divide a region with a given number of orientations further according to the orientation estimates.

ACKNOWLEDGEMENTS

The authors gratefully acknowledge funding of this work by the Deutsche Forschungsgemeinschaft (DFG, AA5/3-1).

REFERENCES

Aach, T., Kaup, A., and Mester, R. (1995). On texture analysis: Local energy transforms versus quadrature filters. *Signal Process*, 45:173–181.

Aach, T., Mota, C., Stuke, I., Mühlich, M., and Barth, E. (2006). Analysis of superimposed oriented patterns. *IEEE Transactions on Image Processing*, 15(12):3690–3700.

Besag, J. (1974). Spatial interaction and the statistical analysis of lattice systems. *Journal Royal Statistical Society B*, 36(2):192–236.

Besag, J. (1986). On the statistical analysis of dirty pictures. *Journal Royal Statistical Society B*, 48(3):259–302.

Bezdek, J. C. (1981). *Pattern Recognition with Fuzzy Objective Function Algorithms (Modern Perspectives in Energy)*. Springer Verlag.

Bigün, J. and Granlund, G. H. (1987). Optimal orientation detection of linear symmetry. In *ICCV87*, pages 433 –438.

Bigün, J., Granlund, G. H., and J.Wiklund (1991). Multidimensional orientation estimation with applications to texture analysis and optical flow. *IEEE Transactions on Pattern Analysis and Machine Intelligence*, 13(8):775–790.

Boykov, Y., Veksler, O., and Zabih, R. (2001). Fast approximate energy minimization via graph cuts. *IEEE Transactions on Pattern Analysis and Machine Intelligence*, 23(11):1222 – 1239.

Derin, H. and Cole, W. S. (1986). Segmentation of textured images using Gibbs random fields. *Computer Vision, Graphics, and Image Processing*, 35:72–98.

Felsberg, M. and Granlund, G. H. (2004). Poi detection using channel clustering and the 2d energy tensor. In *DAGM*, pages 103–110. Springer Verlag.

Frakes, W. (1992). *Information Retrieval Data Structure & Algorithms*. Prentice-Hall, Inc.

Freeman, W. and Adelson, E. (1991). The design and use of steerable filters. *IEEE Trans. PAMI*, 13(9):891–906.

Förstner, W. (1986). A feature based corresponding algorithm for image matching. *Intl. Arch. of Photogrammetry and Remote Sensing*, 26:150–166.

Granlund, G. H. and Knutsson, H. (1995). *Signal Processing for Computer Vision*. Dordrecht, The Netherlands:Kluwer.

Haralick, R. M. (1983). Decision making in context. *IEEE Transactions on Pattern Analysis and Machine Intelligence*, 5(4):417–429.

Jacob, M. and Unser, M. (2004). Design of steerable filters for feature detection using Canny-like criteria. *IEEE Transactions on Pattern Analysis and Machine Intelligence*, 26(8):1007–1019.

Jain, A. K. and Farrokhnia, F. (1991). Unsupervised texture segmentation using Gabor filters. *Pattern Recognition*, 24(12):1167–1186.

Kass, M. and Witkin, A. (1987). Analyzing oriented patterns. *Comput. Vis., Graph., Image Process.*, 37:362–385.

Knutsson, H. and Granlund, G. H. (1983). Texture analysis using two-dimensional quadrature filters. In *IEEE Workshop on Computer Architecure for Pattern Analysis and Image Data Base Management*, Pasadena, CA.

Köthe, U. (2003). Integrated edge and junction detection with the boundary tensor. In *ICCV*, volume 1, pages 424–431.

Lategahn, H., Groß, S., Stehle, T., and Aach, T. (2010). Texture classification by modeling joint distributions of local patterns with gaussian mixtures. *IEEE Transactions on Image Processing*, 19(6):1548–1557.

Lazebnik, S., Schmid, C., and Ponce, J. (2005). A sparse texture representation using local affine regions. *IEEE Transactions on Pattern Analysis and Machine Intelligence*, 27:1265–1278.

Liu, X. and Wang, D. (2003). Texture classification using spectral histograms. *IEEE Transactions on Image Processing*, 12(6):661–670.

Mühlich, M. and Aach, T. (2009). Analysis of multiple orientations. *IEEE Transactions on Image Processing*, 18(7):1424–1437.

Mühlich, M., Friedrich, D., and Aach, T. (2012). Design and implementation of multi-steerable matched filters. *IEEE Transactions on Pattern Analysis and Machine Intelligence*, 34(2):279–291.

Potts, R. (1952). Some generalized order-disorder transformation. *Proc. Cambridge Philosophical Soc.*, 48:106–109.

Randen, T. and Husoy, J. H. (1999a). Filtering for texture classification: A comparative study. *IEEE Transactions on Pattern Analysis and Machine Intelligence*, 21(4):291–309.

Randen, T. and Husoy, J. H. (1999b). Texture segmentation using filters with optimized energy separation. *IEEE Transactions on Image Processing*, 8(4):571–582.

Zenzo, S. D. (1986). A note on the gradient of a multi-image. *Comput. Vis., Graph., Image Process.*, 33:116–125.